

Dependence of the photoluminescence properties of Eu^{2+} doped M-Si-N (M = alkali, alkaline earth or rare earth metal) nitridosilicates on their structure and composition

Ten Kate, Otmar M.; Zhang, Zhijun; Van Ommen, J. Ruud; Hintzen, H. T.

DOI

[10.1039/c8tc00885j](https://doi.org/10.1039/c8tc00885j)

Publication date

2018

Document Version

Final published version

Published in

Journal of Materials Chemistry C

Citation (APA)

Ten Kate, O. M., Zhang, Z., Van Ommen, J. R., & Hintzen, H. T. (2018). Dependence of the photoluminescence properties of Eu^{2+} doped M-Si-N (M = alkali, alkaline earth or rare earth metal) nitridosilicates on their structure and composition. *Journal of Materials Chemistry C*, 6(21), 5671-5683. <https://doi.org/10.1039/c8tc00885j>

Important note

To cite this publication, please use the final published version (if applicable). Please check the document version above.

Copyright

Other than for strictly personal use, it is not permitted to download, forward or distribute the text or part of it, without the consent of the author(s) and/or copyright holder(s), unless the work is under an open content license such as Creative Commons.

Takedown policy

Please contact us and provide details if you believe this document breaches copyrights. We will remove access to the work immediately and investigate your claim.

Cite this: *J. Mater. Chem. C*, 2018,
6, 5671

Dependence of the photoluminescence properties of Eu^{2+} doped M-Si-N ($\text{M} = \text{alkali, alkaline earth or rare earth metal}$) nitridosilicates on their structure and composition†

Otmar M. ten Kate,^a Zhijun Zhang,^b J. Ruud van Ommen^a and
H. T. (Bert) Hintzen^c

Optical data of the Eu^{2+} doped nitridosilicates ($\text{M}_x\text{Si}_y\text{N}_z$) have been collected from the literature and have been analysed with regard to their dependence on structure and composition. Nitridosilicates with a higher degree of condensation, *i.e.* a higher Si/N ratio, generally have a higher Eu^{2+} 4f–5d absorption energy, a higher 5d–4f emission energy and a larger Stokes shift. The higher absorption and emission energies are due to the increase of the N by Si coordination number with increasing Si/N ratio. This results in more electrons on N that participate in the bonding with Si, and thus less electrons are available for Eu–N bonding, reducing the covalency of the Eu–N bonds. The lower covalency gives a weaker nephelauxetic effect, reducing the centroid shift of the 5d level. The lowest 4f–5d absorption energy further increases due to the reduction of the crystal field splitting of the 5d levels, as the Eu–N bonds become longer with increasing Si/N ratio. The Stokes shift increases with increasing degree of condensation despite an increase of lattice rigidity, ascribed to a decrease of local rigidity around the Eu^{2+} ion caused by the larger Eu–N bond lengths. Some nitridosilicates show deviations from the general trends attributed to peculiarities in their crystal structure and the way Eu^{2+} is substituted in the lattice. The relationships established in the present work will be helpful for the design and exploration of new Eu^{2+} doped nitride-based luminescent materials for practical applications.

Received 21st February 2018,
Accepted 19th April 2018

DOI: 10.1039/c8tc00885j

rsc.li/materials-c

1. Introduction

The Eu^{2+} doped $\text{M}_x\text{Si}_y\text{N}_z$ nitridosilicate phosphors ($\text{M} = \text{alkali, alkaline earth or rare earth metal}$) have attracted wide interest in research and industry owing to their large structural variety, chemical stability, environmental friendliness, and favourable luminescence properties.^{1–3} The main interest for their application is as UV or blue light excitable conversion phosphors for white light-emitting diodes (LEDs),^{4–7} but they have also been considered for various other applications such as LCD back-lighting,⁸ solar cells⁹ and afterglow applications.^{10,11} Notable examples are $(\text{AE})_2\text{Si}_5\text{N}_8:\text{Eu}^{2+}$ ($\text{AE} = \text{Ca, Sr, Ba}$),^{12,13} $(\text{AE})\text{SiN}_2:\text{Eu}^{2+}$ ($\text{AE} = \text{Ca, Sr, Ba}$),^{14,15} $\text{BaSi}_7\text{N}_{10}:\text{Eu}^{2+}$,¹⁶ $(\text{AE})(\text{RE})\text{Si}_4\text{N}_7:\text{Eu}^{2+}$ ($\text{AE} = \text{Ca, Sr, Ba; RE} = \text{Sc, Y, Lu}$)^{17–21} and $\text{LaSi}_3\text{N}_5:\text{Eu}^{2+}$.²² The compositional range has been further extended by partly substituting Si and N with Al and O, respectively²³ leading to phosphors such as $(\text{AE})\text{Si}_2\text{O}_2\text{N}_2:\text{Eu}^{2+}$ ($\text{AE} = \text{Ca, Sr, Ba}$),²⁴ $\text{CaAlSiN}_3:\text{Eu}^{2+}$,²⁵ $\text{Ca-}\alpha\text{-sialon}:\text{Eu}^{2+}$,^{26,27} $\beta\text{-sialon}:\text{Eu}^{2+}$ ²⁸ and $\text{Ba}_3\text{Si}_6\text{O}_{12}\text{N}_2:\text{Eu}^{2+}$.²⁹

The energy of the Eu^{2+} 4f–5d excitation and 5d–4f emission is strongly dependent on the local environment because the local coordination determines the energy of the centroid shift and crystal field splitting of the 5d levels as well as the Stokes shift of the emission. As a result, the emission colour varies from blue for $\text{SrSi}_6\text{N}_8:\text{Eu}^{2+}$,³⁰ to green for $\text{LaSi}_3\text{N}_5:\text{Eu}^{2+}$,²² yellow for $\text{SrYSi}_4\text{N}_7:\text{Eu}^{2+}$,¹⁸ and red for $\text{SrSiN}_2:\text{Eu}^{2+}$.¹⁴ Apart from the emission wavelength, other optical properties also vary greatly among the nitridosilicate phosphors, such as the band gap of the host material,³¹ the luminescence efficiency and the quenching temperature.

The $\text{M}_x\text{Si}_y\text{N}_z:\text{Eu}^{2+}$ nitridosilicate structures generally consist of a framework of interconnected SiN_4 tetrahedra with the metal ions located in the cavities of the framework and with Eu^{2+} dopants substituted on the M sites. The nitridosilicates are comparable to the oxosilicates that consist of interconnected SiO_4 tetrahedra, but in the oxosilicates, the O atoms are usually

^a Product and Process Engineering, Chemical Engineering, Applied Sciences, Delft University of Technology, Van der Maasweg 9, Delft 2629 HZ, The Netherlands.
E-mail: o.m.tenkate@tudelft.nl

^b School of Materials Science and Technology, Shanghai University, Shanghai, 200444, China

^c Luminescent Materials Group, Radiation Science and Technology, Applied Sciences, Delft University of Technology, Mekelweg 15, Delft 2629 JB, The Netherlands

† Electronic supplementary information (ESI) available. See DOI: 10.1039/c8tc00885j

onefold or twofold coordinated by Si, while in the nitridosilicates, the threefold coordination of N by Si is more common, and N can even be fourfold coordinated by Si.³² This gives the nitridosilicates a much wider range of structures, from highly condensed Si_3N_4 (Si/N ratio is 0.75), to Ca_4SiN_4 with a very low degree of condensation (Si/N ratio is 0.25).

In the past, various authors have commented on the relations between the optical properties of the lanthanide doped nitridosilicate phosphors and their structure or composition.³³ Quanlin Liu and co-workers³⁴ studied, for several (alumino)-nitridosilicates, the relation between the composition of the material and the centroid shift of the 5d levels of Ce^{3+} , obtaining a linear relationship between the inverse square of the cation electronegativity, which depends on the nitridosilicate composition, and the spectroscopic polarizability, which determines the centroid shift of the Ce^{3+} 5d levels. In a subsequent paper, the crystal field splitting of Ce^{3+} and Eu^{2+} in the nitridosilicates was analysed and related to coordination number, and the polyhedron shape and size.³⁵ Onuma *et al.*³⁶ presented a methodology to estimate the luminescence efficiency of Eu^{2+} doped nitridosilicate phosphors based on structural information, showing that phosphors with a higher symmetry around Eu^{2+} tend to have higher luminescence efficiency. Other authors have compared the luminescence properties of various nitridosilicate phosphors using band structure calculations. Examples include $\text{LaSi}_3\text{N}_5:\text{Ce}^{3+}$ and $\text{La}_3\text{Si}_6\text{N}_{11}:\text{Ce}^{3+}$,³⁷ and Eu^{2+} doped narrow band red-emitting nitridosilicate phosphors.³⁸ In addition, Dorenbos collected information on the energy levels of Eu^{2+} and other lanthanides in many inorganic compounds and developed a model relating those energy levels to each other, to the bandgap of the host lattice and to the vacuum level.^{39–42} However, so far, an overall study on the relation between the structure and composition of the nitridosilicates and the photoluminescence properties of Eu^{2+} doped nitridosilicate compounds that takes into account all known phosphors is lacking.

Recently, we reported on the relations between the degree of condensation in the nitridosilicates and their structural and optical properties, such as bond lengths, coordination number and bandgap.³¹ It was found that with increasing degree of condensation, the M–N bonds become longer, which was explained based on the effective charge of nitrogen: with increasing degree of condensation (Si/N ratio), the N by Si coordination number increases, giving the N atom a less negative effective charge, making less electrons available for covalent M–N bonding, resulting in longer M–N bonds. The less negative effective charge of N also lowers the top of the valence band (mainly composed of N orbitals), while the bottom of the conduction band is moved upward in energy by a decrease of the Si–N distance, overall resulting in an increase of the bandgap with increasing Si/N ratio.

In this manuscript, we extend our previous model from the undoped nitridosilicates to the Eu^{2+} doped nitridosilicate phosphors. For this, we have collected information on all Eu^{2+} doped M–Si–N (M = alkali, alkaline earth or rare earth metal) phosphors reported in the literature and have analysed in a systematic way the 4f–5d excitation and 5d–4f emission energy.

This information is then related to structural properties such as the nitrogen coordination number and the degree of cross-linking in the structure, and a model is deduced that explains the observed relationships. This paper is structured as follows: in Section 2, we discuss the theory of Eu^{2+} 4f–5d excitation and 5d–4f emission and the effects that influence the energy of these transitions: the centroid shift, the crystal field splitting and the Stokes shift. In Section 3, an overview of the luminescence properties of all Eu^{2+} doped nitridosilicates published in the literature is given, and subsequently, the photoluminescence properties are evaluated and related to the composition (Si/N ratio) and structural properties (bond length).

2. Eu^{2+} absorption and emission energy

Eu^{2+} doped compounds usually have strong absorption bands in the near UV region and parts of the visible spectrum. These absorption bands are due to excitation of an electron from the 4f ground state to the 5d excited states (4f–5d absorption), changing the electron configuration of Eu^{2+} from $[\text{Xe}]4f^7$ to $[\text{Xe}]4f^65d^1$. The absorption can result in the emission of a photon, usually in the visible part of the spectrum, when the electron returns to the ground state (5d–4f emission). Both the excitation and emission energies strongly vary between different compounds, as the local environment of the Eu^{2+} ions influences the energy differences between the 4f ground state and 5d excited states. The effects that the environment has on the Eu^{2+} 4f–5d absorption and 5d–4f emission can be divided into three parts: the centroid shift (CS), the crystal field splitting (CFS) and the Stokes shift (ΔS), as illustrated in Fig. 1a. We will now discuss the centroid shift and crystal field splitting in Sections 2.1 and 2.2, respectively, and the combined effect on the lowest 5d (*i.e.* the redshift) level in Section 2.3. In Section 2.4, the Stokes shift will be discussed and in Section 2.5, the width of the emission band will be discussed.

2.1 Centroid shift

When Eu^{2+} is incorporated in a compound, the centre of gravity (barycentre) of the 5d levels is lowered as compared to the free Eu^{2+} ion in vacuum, reducing the energy difference between the 4f ground state and 5d excited states. This decrease of the

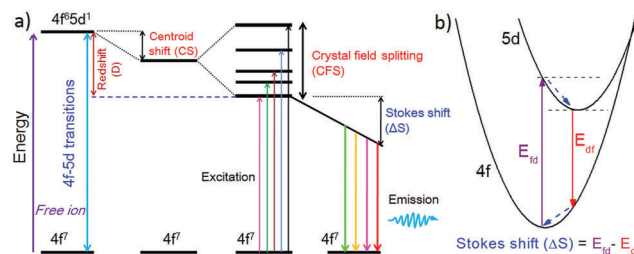


Fig. 1 (a) Diagram of the shift in energy between the Eu^{2+} 4f ground state and the 5d levels caused by the centroid shift and the crystal field splitting, and the lowering of the 5d–4f emission energy by the Stokes shift; (b) configurational coordinate diagram, showing Eu^{2+} 4f–5d excitation, relaxation and 5d–4f emission.

barycentre of the 5d levels is called the centroid shift and it is the result of the expansion of the 5d orbitals of Eu^{2+} due to the covalent bonding between Eu^{2+} and its coordinating anions (the nephelauxetic effect),^{43,44} which reduces the energy of the 5d levels. The nephelauxetic effect becomes stronger if the anions involved are less electronegative, because this will make the Eu–X (X = anion) bonds more covalent. In addition, the effect becomes stronger with increasing anion polarizability^{45,46} as the correlated motion of the 5d electron with the electrons of the anions increases the covalency. The nephelauxetic effect is in general relatively weak for fluorides, somewhat stronger for oxides, and even stronger for nitrides, as N^{3-} has a lower electronegativity and higher spectroscopic polarizability than O^{2-} and in particular F^- .

2.2 Crystal field splitting

Apart from causing a centroid shift, the surrounding anions have an additional influence on the $\text{Eu}^{2+} 4f^6 5d^1$ state: crystal field splitting (CFS). The 5d electron and the electrons in the neighbouring anions repel each other, which gives a 5d electron in an orbital that is oriented towards an anion ligand a higher energy, and a 5d electron in an orbital that is oriented towards a position in between the ligands a lower energy. The result is an energy splitting (the crystal field splitting) of the 5d levels with the same energy into at most five levels with different energy, depending on the local site symmetry. The size of the energy splitting depends on the crystal field strength, which is larger if the Eu–X (X = anion) distance is shorter. In addition, the symmetry of the anions around the Eu^{2+} ion also strongly influences the CFS, decreasing in size when going from octahedral environments (6-fold coordination) towards environments with larger coordination numbers.⁴⁷ If the separate 5d bands can be observed in an excitation spectrum, the size of the CFS can be estimated by the energy difference between the highest energy (E_{5d_5}) and lowest energy 5d band (E_{5d_1}):

$$\text{CFS (eV)} = E_{5d_5} - E_{5d_1} \quad (1)$$

The average energy of the bands can be used to estimate the centroid energy (CE) between the 4f ground state and the 5d barycentre, from which the centroid shift (CS) of the Eu^{2+} 5d levels can be calculated:

$$\text{CS (eV)} = 4.93 \text{ eV} - \text{CE} = 4.93 \text{ eV} - 0.2(E_{5d_1} + E_{5d_2} + E_{5d_3} + E_{5d_4} + E_{5d_5}) \quad (2)$$

Here, 4.93 eV is the barycentre energy for the $4f^6 5d^1$ levels of the free Eu^{2+} ion in vacuum.⁴¹ Note that the calculations for the CS and the CFS are only approximate and assume an equidistant energy distribution of the five 5d energies. The exact splitting of the 5d levels is dependent on the symmetry around Eu^{2+} . It is, however, believed that the approximation is good enough to observe the correct general trends.

2.3 Redshift

In practice, it can be difficult to study the effect of the centroid shift and the crystal field splitting of the Eu^{2+} 5d levels separately.

The 5d bands are broad and partly overlap and the higher energy bands may be hidden by the host lattice absorption, making it impossible to determine the exact positions of the separate 5d bands necessary for determining the position of the 5d barycentre and the size of the crystal field splitting. For comparison between different Eu^{2+} doped compounds, one can therefore consider the combined effect of the centroid shift and the crystal field splitting on the energy of the lowest 5d state. This combined effect is called the redshift D and, by definition, the redshift is equal to the energy of the lowest 4f–5d transition of Eu^{2+} in vacuum (4.22 eV) minus the energy of the lowest 4f–5d transition in the compound (E_{fd}):³⁹

$$D \text{ (eV)} = 4.22 \text{ eV} - E_{fd} \quad (3)$$

For the determination of E_{fd} , one should realize that one cannot simply, as is sometimes done, take the first maximum at the low energy side of the excitation spectrum. The lowest energy state of the $4f^6 5d^1$ configuration is the $4f^6[{}^7F_0]5d^1$ state. In some favourable cases (at low temperature and low Eu concentrations), the energy difference between the $\text{Eu}^{2+} 4f^7$ ground state and the $4f^6[{}^7F_0]5d^1$ state can be observed directly in the excitation spectra as a separate peak at the long wavelength side of the excitation band, but in most cases, it cannot be resolved separately. In those cases, E_{fd} can be quite well estimated from the luminescence excitation spectrum by taking the value at the low energy side of the first maximum of the 5d bands where the intensity has dropped to 15–20%,⁴⁸ which is also the approach that is used in this manuscript. As another approximation, other authors sometimes estimate E_{fd} as the cross-section between the normalized excitation and emission spectra, which leads to similar values.

2.4 Stokes shift

After excitation of an electron from the 4f to the 5d state, relaxation will occur to the lowest 5d level. From there, the electron may return to the 4f ground state accompanied by the emission of a photon. As a result of relaxations, illustrated by the configurational coordinate diagram in Fig. 1b, the energy of emission E_{dr} is usually at lower energy than the lowest absorption transition E_{fd} . The difference in energy is called the Stokes shift ΔS . The size of the Stokes shift thus depends on the degree of relaxation of excited Eu^{2+} in the lattice, and is therefore sometimes related to the lattice rigidity. This is, for instance, reflected when comparing the smaller Stokes shift in rigid crystalline host lattices with the larger Stokes shift in less rigid glassy samples of the same composition.⁴⁹ The Stokes shift also tends to be larger if Eu^{2+} is substituted on a smaller cation site because Eu^{2+} tends to shrink as a consequence of 4f–5d excitation and this shrinkage is not constrained when Eu^{2+} is located on a smaller site.⁵⁰ On the other hand, a lattice with smaller cations of higher charge (such as Si^{4+}) will be more rigid, making shrinkage more difficult,⁵⁰ and consequently, the Stokes shift will be smaller. It should be noted that in this manuscript, the Stokes shift is defined as the energy difference between the $4f^6[{}^7F_0]5d^1$ excited state (E_{fd}) and the maximum of the 5d–4f emission band (E_{dr}), but other authors sometimes

define the Stokes shift as the energy difference between the maxima of the excitation and emission bands, resulting in a systematically larger Stokes shift. This is the reason that the Stokes shift determined in this work may deviate from the value given in the publication from which the data were obtained.

2.5 Emission band width

The width of the Eu^{2+} 5d–4f emission band varies from compound to compound. The relation between the full-width at half maximum (FWHM) of the Eu^{2+} 5d–4f emission band and the Stokes shift ΔS can be approximated using the Huang–Rhys parameter S and the phonon energy of the lattice $\hbar\omega$, which are related to the Frank–Condon offset and the curvature of the parabola in the configurational diagram according to the formula:^{39,51}

$$\text{FWHM} = 2.36\hbar\omega \sqrt{S \coth\left(\frac{\hbar\omega}{2kT}\right)} \text{ with } S = 0.5\left(\frac{\Delta S}{\hbar\omega} + 1\right) \quad (4)$$

which assumes that the ground state and excited state parabola have the same curvature. Here, k is the Boltzmann constant and T is the absolute temperature. Following the equation, this shows that in general, the emission band width becomes larger if the Stokes shift increases, *i.e.* if Eu^{2+} relaxes more easily. In addition to the relaxation, the total emission band will also be broad, as well as asymmetrically shaped, if Eu^{2+} ions are present in multiple different local environments, as the total emission band will then be a combination of multiple bands. The band width is especially important for red-emitting phosphors, as broad emission bands will have part of their emission at very long wavelengths for which the human eye is not or only weakly sensitive, making narrow band emission phosphors more desired.⁵²

3. Eu^{2+} absorption and emission energy in the nitridosilicates

In this study, we consider all nitridosilicate phosphors with the general composition $\text{M}_x\text{Si}_y\text{N}_z$ for which Eu^{2+} doping has been reported. Information on the range and relationship between x , y and z can be found in the ESI.† The luminescence properties of these phosphors are listed in Table 1. The values have been derived from experimental data reported in the literature, using the methods discussed in Section 2. Note that we limit ourselves to samples with a low Eu^{2+} concentration (around 1 mol%), because this makes the different compounds more comparable and because there is less Eu–Eu energy transfer and reabsorption at low Eu concentrations. We have assumed that Eu is substituted in the lattice on the M sites, unless indicated otherwise in the literature. The Li and Mg containing nitridosilicates such as LiSi_2N_3 , $\text{Li}_4\text{Ca}_3\text{Si}_2\text{N}_6$, MgSiN_2 and $\text{SrMg}_3\text{SiN}_4$ have also been included, even though it may be argued that some of these compounds are not really nitridosilicates but nitrido-lithosilicates or nitrido-magnesosilicates because Li and Mg form TN_4 ($T = \text{Mg}, \text{Li}$) tetrahedra like SiN_4 tetrahedra and are therefore sometimes considered to be a part of the nitridosilicate framework. In those cases, one could argue that the degree of condensation (κ) should

be defined as the $(\text{Si} + \text{Mg} + \text{Li})/\text{N}$ ratio instead of Si/N ratio. However, Li and Mg are not considered part of the framework in all compounds. In addition, Mg and Li have a different size and oxidation state than Si, so Mg and Li will have a different quantitative influence than Si on the physical properties. Therefore, we use the Si/N ratio and not the $(\text{Si} + \text{Mg} + \text{Li})/\text{N}$ ratio as the parameter to describe the degree of condensation. A strong deviation of certain trends for Li and Mg containing materials can then be seen as a possible indication that Li and Mg are part of the Si–N network affecting the properties. An overview of the structural information of the nitridosilicates can be found in our previous publication.³¹

The Eu^{2+} 4f–5d absorption and 5d–4f emission energies listed in Table 1 have an uncertainty of about 0.1 eV. The errors for the positions of the 5d bands, and consequently also for the centroid shift (CS) and crystal field splitting (CFS), are somewhat larger, because the positions of the 5d bands are often not well resolved, as explained in Section 2.3. Therefore, the 5d bands are only listed for a limited number of compounds, as for other compounds, not enough information is available in order to reliably determine their positions, as sometimes the highest energy 5d bands can be hidden by the host lattice absorption.

3.1 Eu^{2+} 4f–5d absorption

Fig. 2 shows that the energy E_{fd} of the lowest Eu^{2+} 4f–5d transition in the nitridosilicates tends to increase (and that the redshift D tends to decrease) if the structures become more condensed (*i.e.* have a higher Si/N ratio). E_{fd} increases from 1.40 eV for $\text{CaLaSiN}_3:\text{Eu}^{2+}$ with a low Si/N ratio, to 3.19 eV for $\text{BaSi}_3\text{N}_{10}:\text{Eu}^{2+}$ with a high Si/N ratio. E_{fd} should also be quite low for $\text{Ca}_4\text{SiN}_4:\text{Eu}^{2+}$ (low Si/N ratio of 0.25) considering its low energy emission of 1.71 eV, but its excitation spectrum has not been reported. Note that the linear fit through the data in Fig. 2 does not imply that the relation between E_{fd} and the Si/N ratio should actually be linear. The purpose of the fit is to indicate the upward trend of E_{fd} with increasing Si/N ratio and it is helpful in order to identify exceptions to the general trend.

One of the main exceptions to the trend is the E_{fd} of $\text{Li}_4\text{Ca}_3\text{Si}_2\text{N}_6:\text{Eu}^{2+}$ (3.54 eV), which is much higher than that of the other nitridosilicates with similar Si/N ratios. It is probably wrongly interpreted as it would also mean that the material has an abnormally large Stokes shift of 1.76 eV. It is more likely that the excitation band that was reported to be the Eu^{2+} 4f–5d transition⁵³ has a different origin. On the other hand, the E_{fd} of $\text{CaLaSiN}_3:\text{Eu}^{2+}$ is relatively low, but one should consider that the E_{fd} of $\text{CaLaSiN}_3:\text{Eu}^{2+}$ has been determined differently than the E_{fd} of the other compounds as Eu^{2+} 5d–4f emission is not observed in Eu^{2+} doped CaLaSiN_3 and consequently, an excitation spectrum cannot be measured.⁵⁴ E_{fd} of $\text{CaLaSiN}_3:\text{Eu}^{2+}$ was therefore obtained from an absorption spectrum instead of an excitation spectrum.⁵⁴

The redshift D , which is determined by E_{fd} (eqn (3), Section 2.3), is the result of the combined effects of the centroid shift (CS) and the crystal field splitting (CFS). The centroid shift of the Eu^{2+} 5d level can be estimated from the average position of the 5d bands (eqn (2), Section 2.2), and it is listed in Table 1.

Table 1 Luminescence properties of the Eu^{2+} doped nitridosilicates ($\text{M}_x\text{Si}_y\text{N}_z$), showing the lowest 4f–5d transition E_{fd} (column 2), the positions of the 5d bands (column 3), the 5d centroid shift CS (column 4), the 5d crystal field splitting CFS (column 5), the 5d–4f emission maximum E_{df} (column 6), the Stokes shift ΔS (column 7), and the full width at half maximum (FWHM) of the emission band (column 8)

Compound	E_{fd} (eV)	5d bands (nm)	CS (eV)	CFS (eV)	E_{df} (eV)	ΔS (eV)	FWHM (eV)	Ref.
$\alpha\text{-Si}_3\text{N}_4$	2.90	266, 293, 331, 370, 410	1.13	1.64	2.61	0.29	0.64	55
$\beta\text{-Si}_3\text{N}_4$	2.56				2.26	0.30	0.31	55–57
LiSi_2N_3	2.76	257, 298, 352, 414	1.05	1.83	2.25	0.51	0.40	58–62
MgSiN_2	3.00				2.39	0.61	0.60	63–65
Ca_4SiN_4					1.71			66
$\text{Ca}_5\text{Si}_2\text{N}_6$	2.30				2.04	0.26	0.39	67
$\alpha\text{-CaSiN}_2$	2.16	305, 350, 409, 479, 532	1.82	1.73	1.97	0.19	0.37	15
$\text{Ca}_{16}\text{Si}_{17}\text{N}_{34}$ (high energy site) ^a					2.07		2.07	68 and 69
$\text{Ca}_{16}\text{Si}_{17}\text{N}_{34}$ (intermediate) ^a					1.94		1.94	68 and 69
$\text{Ca}_{16}\text{Si}_{17}\text{N}_{34}$ (low energy site) ^a	2.15	300, 375, 405, 475	1.65	1.52	1.81	0.34	1.08	68 and 69
$\text{Ca}_2\text{Si}_5\text{N}_8$ (high energy site)					2.05		0.22	13 and 70–72
$\text{Ca}_2\text{Si}_5\text{N}_8$ (low energy site)	2.30	297, 355, 394, 460	1.52	1.48	1.88	0.42	0.32	13 and 70–72
$\text{HP-Ca}_2\text{Si}_5\text{N}_8$	2.30	320, 355, 390, 470	1.67	1.24	1.98	0.32	0.31	73
SrSiN_2	2.33	306, 336, 395, 466	1.54	1.39	1.87	0.46	0.36	14 and 74
$\text{Sr}_2\text{Si}_5\text{N}_8$ (high energy site)					2.05		0.23	13 and 70–72
$\text{Sr}_2\text{Si}_5\text{N}_8$ (low energy site)	2.20	294, 334, 395, 465	1.49	1.49	1.88	0.32	0.29	13 and 70–72
SrSi_6N_8	2.89				2.72	0.17	0.28	30
BaSiN_2	2.38	312, 334, 395, 464	1.64	1.30	2.07	0.31	0.34	14
$\text{Ba}_2\text{Si}_5\text{N}_8$ (high energy site)					2.14		0.21	13, 70–72 and 75
$\text{Ba}_2\text{Si}_5\text{N}_8$ (low energy site)	2.30	295, 334, 395, 460	1.56	1.48	1.97	0.33	0.31	13, 70–72 and 75
$\text{BaSi}_7\text{N}_{10}$	3.19	286, 332	0.97	0.45	2.61	0.58	0.46	16 and 76
BaSi_6N_8	2.99				2.76	0.23	0.25	77
$\text{SrMg}_3\text{SiN}_4$	2.18	370, 450, 510	2.08	0.92	2.04	0.14	0.17	78
$\text{BaMg}_3\text{SiN}_4$	2.18	405, 470, 525	2.24	0.70	1.85	0.33	0.26	79
LaSi_3N_5	2.70	340, 374, 440	1.70	0.94	2.30	0.40	0.40	80 and 81
$\text{Li}_4\text{Ca}_3\text{Si}_2\text{N}_6$	(3.54) ^b				1.75	(1.76) ^b	0.17	53
$\text{Li}_2\text{CaSi}_2\text{N}_4$					2.12		0.26	82
$\text{Li}_2\text{SrSi}_2\text{N}_4$	2.38				2.02	0.36	0.27	82
$\text{Li}_2\text{Ca}_2\text{Mg}_2\text{Si}_2\text{N}_6$	2.10				1.94	0.16	0.16	83 and 84
$\text{Ca}_3\text{MgLi}_2\text{Si}_2\text{N}_6$	1.97				1.69	0.28	0.31	85
CaLaSiN_3	1.40 ^c				^c	^c	^c	54
$\text{CaScSi}_4\text{N}_7$	2.76	310, 380	1.32	0.53	2.34	0.42	0.39	20
$\text{SrScSi}_4\text{N}_7$	2.76	310, 380	1.32	0.53	2.36	0.40	0.37	20 and 86
$\text{BaScSi}_4\text{N}_7$	2.73	315, 375	1.31	0.63	2.36	0.37	0.37	20
CaYSi_4N_7 ($\text{Ca}_{0.8}\text{Y}_{1.2}\text{Si}_4\text{N}_{6.8}\text{C}_{0.2}$)	2.82	340, 385	1.50	0.43	2.19	0.63	0.68	19
SrYSi_4N_7	2.79	340, 385	1.50	0.43	2.24	0.55	0.49	18–21 and 87
BaYSi_4N_7	2.80	348, 385	1.54	0.34	2.35	0.45	0.43	17, 19 and 21
$\text{SrLuSi}_4\text{N}_7$	2.85	340, 370, 390	1.54	0.45	2.34	0.51	0.45	21
$\text{BaLuSi}_4\text{N}_7$	2.85	340, 370, 390	1.54	0.45	2.34	0.51	0.45	21
$\text{CaLaSi}_4\text{N}_7$	2.30				1.99	0.31	0.32	88

^a $\text{Ca}_{16}\text{Si}_{17}\text{N}_{34}$ is also called cubic- CaSiN_2 . ^b E_{fd} of $\text{Li}_4\text{Ca}_3\text{Si}_2\text{N}_6\text{:Eu}^{2+}$, and consequently the Stokes shift, might be incorrect as is discussed in the main text. ^c No Eu^{2+} 5d–4f emission has been observed for $\text{CaLaSiN}_3\text{:Eu}^{2+}$, therefore E_{fd} has been derived from an absorption spectrum.

The CS (Fig. 3a) shows a strong decrease with increasing Si/N ratio, from over 2.2 eV for $\text{BaMg}_3\text{SiN}_4\text{:Eu}^{2+}$ with a low Si/N ratio to less than 1.0 eV for $\text{BaSi}_7\text{N}_{10}\text{:Eu}^{2+}$ with a high Si/N ratio. There are no significant exceptions to this trend as for all compounds in Fig. 3a, the CS deviates by less than 0.25 eV from the trend line. It should, however, be noted that not all Eu^{2+} doped compounds are shown in Fig. 3a as, for some compounds, the CS could not be determined.

The smaller centroid shift with increasing Si/N ratio can be understood by considering the coordination number of N by Si. With increasing degree of condensation (increasing Si/N ratio, κ) for the nitridosilicates, the average coordination number of N by Si (x) increases, according to the relation $x = 4 \times \kappa$.³¹ As a result, more electrons of N will participate in the bonding with Si (as a result, the Si–N bond lengths also decrease)³¹ and thus less electrons will be available for bonding with Eu. Hence, the Eu–N bonds become less covalent with increasing degree of

condensation, resulting in a weaker nephelauxetic effect and thus a smaller centroid shift. Note that this explanation does not take into account certain local effects such as variations in Eu by N coordination number, deviations from ideal SiN_4 tetrahedral symmetry, or that the actual N by Si coordination number for the N atoms surrounding Eu may be different from the average N by Si coordination number. A perfect correlation between the centroid shift and the Si/N ratio would therefore also not be expected, apart from whether it is linear or not. Nevertheless, the scattering around the general trend in Fig. 3a is only small (up to 0.2 eV) and the Si/N ratio can be considered a principle parameter. Note that $\text{LaSi}_3\text{N}_5\text{:Eu}^{2+}$, $\text{LiSi}_2\text{N}_3\text{:Eu}^{2+}$ and $\alpha\text{-Si}_3\text{N}_4\text{:Eu}^{2+}$ do not deviate significantly from the main trend, even though Eu^{2+} cannot substitute on a divalent M site in these lattices and therefore some form of charge compensation needs to be present. Apparently, these charge compensation effects do not have a significant influence on the energy of the centroid shift.

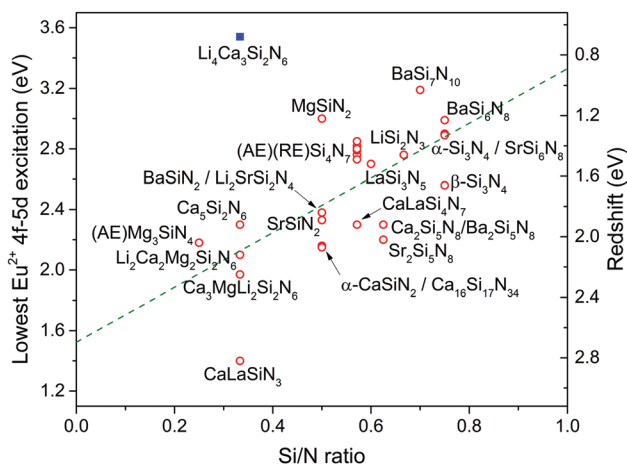


Fig. 2 Energy of the lowest Eu^{2+} 4f–5d transition (E_{fd}) versus the Si/N ratio (κ) of the Eu^{2+} doped nitridosilicates. The dashed green line is a linear fit through the red data points in order to indicate the trend. More details on the fit can be found in the ESI.† The data points for $(\text{AE})\text{Mg}_3\text{SiN}_4:\text{Eu}^{2+}$ (AE = Sr, Ba), as well as those of $(\text{AE})(\text{RE})\text{Si}_4\text{N}_7:\text{Eu}^{2+}$ (AE = Ca, Sr, Ba; RE = Sc, Y, Lu), are close together and therefore not indicated with separate labels for each compound.

The strength of the crystal field splitting (CFS) of the Eu^{2+} 5d levels can be estimated from the energy difference between the highest and lowest energy 5d band (eqn (1), Section 2.2). For the crystal field splitting in the Eu^{2+} doped nitridosilicates, listed in Table 1, there is not a clear correlation with the Si/N ratio (Fig. 3b). The CFS is, for example, small for $\text{BaSi}_7\text{N}_{10}:\text{Eu}^{2+}$ (0.46 eV) but large for $\alpha\text{-Si}_3\text{N}_4:\text{Eu}^{2+}$ (1.64 eV) while both have a high Si/N ratio (0.7–0.75 eV). The CFS is also much larger for the $(\text{AE})\text{SiN}_2:\text{Eu}^{2+}$ compounds than for the $(\text{AE})(\text{RE})\text{Si}_4\text{N}_7:\text{Eu}^{2+}$ compounds, while the difference in Si/N ratio is only small. That there is no clear correlation may not be so surprising, considering that the crystal field splitting is strongly dependent on the size and shape (symmetry) of the coordinating anion polyhedron around Eu^{2+} as determined by the crystal structure, as was shown by Wang *et al.*³⁵ for the Eu^{2+} and Ce^{3+} doped nitridosilicates, and more generally for inorganic compounds by Dorenbos.⁴⁷ Note that, although there is not a clear correlation between CFS and Si/N ratio, there is still quite a good correlation between the redshift and the Si/N ratio (Fig. 2), even though the redshift depends on the CFS. The reason for this is that the correlation between the redshift and the Si/N ratio is mainly due to the centroid shift, which has a larger contribution to the redshift than the CFS, as only about half of the CFS contributes to the redshift.

In Fig. 4a, the lowest energy 4f–5d transition (E_{fd}) is shown versus the average distance from Eu^{2+} to the coordinating N^{3-} anions. The Eu–N distances are derived from the M–N distances obtained from crystallographic data of the undoped compounds, summarized in our previous publication.³¹ When Eu is substituted on an M site, the distances to the anions change because of the size difference between Eu and M, as Eu^{2+} is larger than, for example, Ca^{2+} and smaller than, for example, Ba^{2+} . In order to take these changes into account, the average distance ($R_{\text{M-N}}$) is

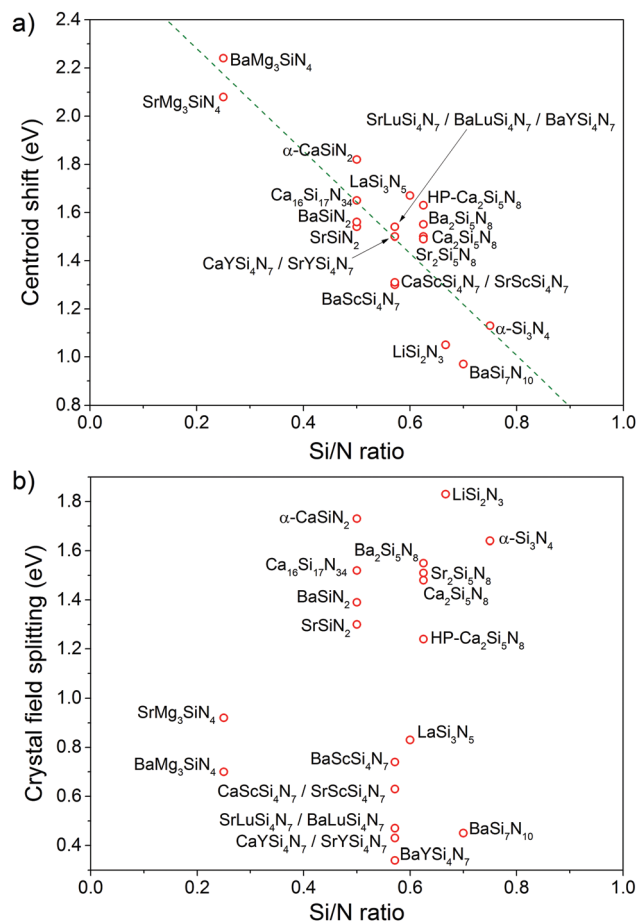


Fig. 3 (a) Centroid shift (CS) and (b) crystal field splitting (CFS) energy versus the Si/N ratio (κ) in the Eu^{2+} doped nitridosilicates. The dashed green line is a linear fit through the red data points in order to indicate the trend. More details on the fit can be found in the ESI.†

corrected for the size difference between Eu^{2+} and the cation M for which it substitutes, using the equation:⁴¹

$$R_{\text{Eu-N}} = R_{\text{M-N}} + \Delta R = R_{\text{M-N}} + f \times (r_{\text{M}} - r_{\text{Eu}}) \quad (5)$$

Here, $R_{\text{Eu-N}}$ is the average Eu–N distance, $R_{\text{M-N}}$ is the average M–N distance in the undoped compound according to the literature, ΔR is the compensation term and f is a scaling factor, which is set to 0.6, following ref. 89. r_{Eu} and r_{M} are the ionic radii of Eu^{2+} ion and the cation M (according to Shannon⁹⁰) for which it substitutes, respectively. In some compounds, there are two or more crystallographically different M sites on which the Eu^{2+} ions can be substituted. In those compounds where there are divalent as well as monovalent or trivalent sites, it was assumed that Eu^{2+} substitutes on the divalent site. In those cases where there are multiple sites of the same valence, the average of the multiple sites was taken, unless there is some indication from the reported luminescence data that the luminescence can be assigned to a specific site, as is the case for $(\text{AE})_2\text{Si}_5\text{N}_8:\text{Eu}^{2+}$ (AE = Ca, Sr, Ba)⁷⁰ and $\text{Ca}_{16}\text{Si}_{17}\text{N}_{34}:\text{Eu}^{2+}$.⁶⁹ The emission from these phosphors occurs from Eu^{2+} substituted on multiple AE sites and the observed E_{fd} is assigned to

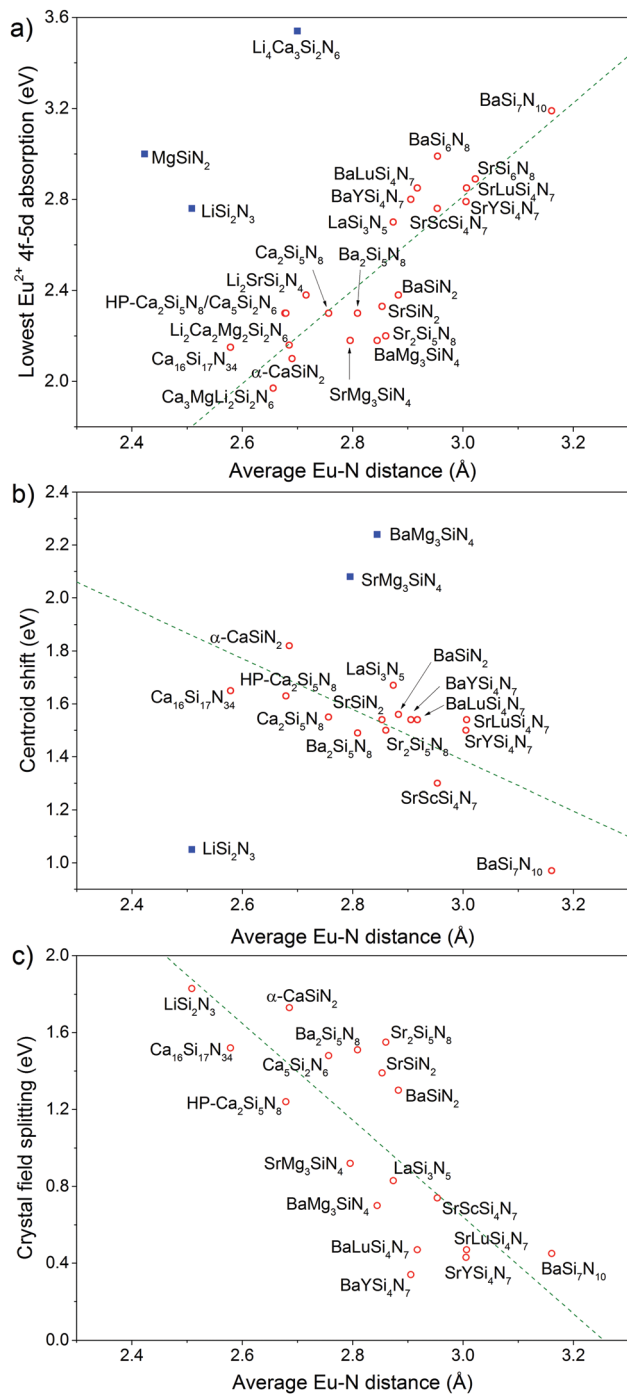


Fig. 4 Energy of (a) the lowest 4f–5d transition (E_{fd}), (b) the centroid shift (CS) and (c) the crystal field splitting (CFS) of Eu^{2+} in the nitridosilicates versus the average Eu–N distance (R_{Eu-N}). The dashed green lines are linear fits through the red data points in order to indicate the trend. More details on the fits can be found in the ESI.†

the lowest energy site. The E_{fd} from the higher energy sites is hidden in the excitation spectra.

Fig. 4a shows a good correlation between E_{fd} and the average Eu–N distance: the larger the bond lengths, the larger the E_{fd} . This is in accordance with the observation that E_{fd} increases with increasing Si/N ratio (Fig. 2) and that the Eu–N distance

also increases with increasing Si/N ratio (see Fig. 4 in ref. 31). This can also be understood in terms of both the nephelauxetic effect and the crystal field splitting: the larger the distance between Eu and the coordinating N anion, the weaker the nephelauxetic effect and the smaller the crystal field splitting, resulting in a higher E_{fd} . This is confirmed by Fig. 4b and c, showing a decrease of the centroid shift (i.e. a decrease of the nephelauxetic effect) and a decrease of the crystal field splitting with increasing Eu–N distance. Most values in Fig. 4a fall within a range of 0.3 eV from the fitted trend line. However, three compounds deviate significantly from the general trend: $LiSi_2N_3:Eu^{2+}$, $MgSiN_2:Eu^{2+}$ and $Li_4Ca_3Si_2N_6:Eu^{2+}$. For $LiSi_2N_3:Eu^{2+}$ and $MgSiN_2:Eu^{2+}$, this may indicate that Eu^{2+} is not located on the small Li or Mg sites. These sites are so small that Eu^{2+} might be too large to fit on those sites. Note that the centroid shift for $LiSi_2N_3:Eu^{2+}$ also deviates (Fig. 4b), while the centroid shift for $MgSiN_2:Eu^{2+}$ is not known. For $Li_4Ca_3Si_2N_6:Eu^{2+}$, it is most likely that the excitation band is not correctly interpreted in the original publication⁵³ and that it has a different origin, as was mentioned before. In Fig. 4b, the (AE) $Mg_3SiN_4:Eu^{2+}$ (AE = Sr, Ba) compounds deviate considerably by more than 0.5 eV, but not in Fig. 4a. The reason for the deviation is not exactly clear. It might be related to the presence of Mg in the lattice, but it could also be that the centroid shift has been overestimated and that the crystal field splitting has been underestimated, as it might be that there are 5d bands located at high energy that were not observed because they are hidden by the host lattice absorption. Note that the bandgaps of $SrMg_3SiN_4$ and $BaMg_3SiN_4$ (both 4.1 eV)^{31,78,79} are relatively small.

One can see from Table 1 that E_{fd} hardly depends on AE in (AE) $ScSi_4N_7:Eu^{2+}$ (AE = Ca, Sr, Ba). All these three compounds crystallize in the same crystal structure with the Eu^{2+} ion located on the divalent AE site. The same is observed for other isostructural compounds: also, in (AE) $LuSi_4N_7$ (AE = Sr, Ba), (AE) $YSi_4N_7:Eu^{2+}$ (M = Sr, Ba) and (AE) $Si_5N_8:Eu^{2+}$ (M = Sr, Ba), E_{fd} is nearly independent of AE. The crystal field and nephelauxetic effect around Eu remain almost the same due to the similarities in crystal structure and also the Eu–N distance does not change much: the bonds with N can contract if Eu is substituted on a larger Ba site and can expand if Eu is substituted on a smaller Ca site. Note that E_{fd} may vary for isocompositional compounds if the crystal structure is changing such as in the series (AE) $SiN_2:Eu^{2+}$ (AE = Mg, Ca, Sr, Ba) with four different crystal structures.

3.2 Eu^{2+} 5d–4f emission

Fig. 5 shows that the energy of the Eu^{2+} 5d–4f emission (E_{df}) increases with increasing degree of condensation (Si/N ratio). The emission energy is smallest (around 1.7 eV) for $Ca_4SiN_4:Eu^{2+}$ and $Ca_3MgLi_2Si_2N_6:Eu^{2+}$ with a low Si/N ratio and largest (2.6 eV or higher) for (AE) $Si_6N_8:Eu^{2+}$ (AE = Sr, Ba), $BaSi_7N_{10}:Eu^{2+}$ and $\alpha-Si_3N_4:Eu^{2+}$ with a high Si/N ratio. This trend is similar to the increase of the lowest 4f–5d excitation energy (E_{fd}) with increasing Si/N ratio observed in Fig. 2, due to the decrease of the centroid shift (Fig. 3a) as a result of the less covalent Eu–N bonds. Although there is some scattering around the trend line in

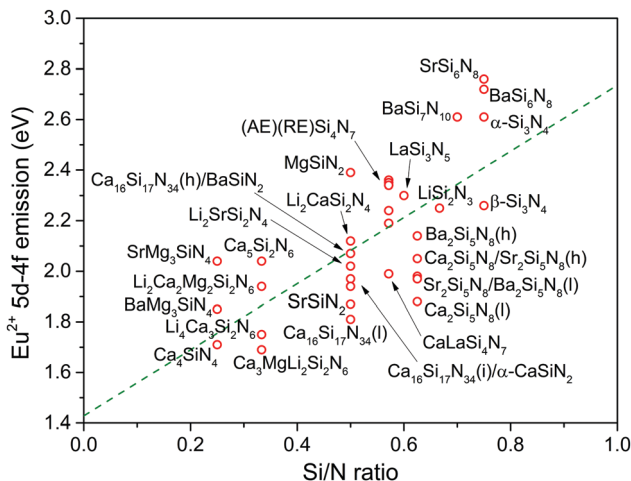


Fig. 5 Eu^{2+} 5d–4f emission energy E_{dif} versus the Si/N ratio (κ) for the Eu^{2+} doped nitridosilicates. The dashed green line is a linear fit through the red data points in order to indicate the trend. More details on the fit can be found in the ESI.† The data points for (AE)(RE) Si_4N_7 : Eu^{2+} (AE = Ca, Sr, Ba; RE = Sc, Y, Lu) are close together and therefore not indicated with separate labels for each compound. The letters (h), (i) and (l) indicate the high, intermediate and low energy emission, respectively.

Fig. 5, none of the compounds shows a very strong deviation (over 0.4 eV) from the general trend. This also holds for $\text{Li}_4\text{Ca}_3\text{Si}_2\text{N}_6$: Eu^{2+} that was strongly deviating in Fig. 2. Apparently, although the 4f–5d absorption energy was probably wrongly interpreted, the observed emission band may indeed have been correctly assigned as Eu^{2+} 5d–4f emission.

The Stokes shift of the Eu^{2+} doped nitridosilicate phosphors is given by the energy difference between the energy of the lowest Eu^{2+} 4f–5d excitation (E_{fd}), shown in Fig. 2, and the energy of the Eu^{2+} 5d–4f emission maximum (E_{dif}), shown in Fig. 5. From Fig. 6a, it can be seen that the Stokes shift tends to increase with increasing degree of condensation (Si/N ratio), although the scattering around the trend line is quite large. The Stokes shift is very small (around 0.15 eV) for $\text{SrMg}_3\text{SiN}_4$: Eu^{2+} and $\text{Li}_2\text{Ca}_2\text{Mg}_2\text{Si}_2\text{N}_6$: Eu^{2+} with a low Si/N ratio, becomes larger (0.2–0.5 eV) for $\text{Ca}_5\text{Si}_2\text{N}_6$: Eu^{2+} and (AE) SiN_2 : Eu^{2+} , and is relatively large (around 0.6 eV) for $\text{BaSi}_7\text{N}_{10}$: Eu^{2+} . Clear exceptions to this trend are α - Si_3N_4 : Eu^{2+} , β - Si_3N_4 : Eu^{2+} and (AE) Si_6N_8 : Eu^{2+} (AE = Sr, Ba), for which the Stokes shift is relatively small, which will be further discussed below.

With increasing degree of condensation, the cross-linking between the SiN_4 tetrahedra in the nitridosilicates increases, which makes the structures more rigid. The increase of structural rigidity with increasing degree of cross-linking can be seen from Fig. 6b, where the Debye temperature is shown versus the degree of condensation (Si/N ratio). The Debye temperature, which is obtained from data collected from the literature (γ - Si_3N_4 ,⁹¹ $\text{La}_3\text{Si}_6\text{N}_{11}$,⁹² $\text{Sr}_2\text{Si}_5\text{N}_8$,⁹³ MgSiN_2 and β - Si_3N_4 ⁹⁴ and other compounds³⁸) is a measure for the lattice rigidity of the structure.⁹⁵ Although the amount of data is limited, Fig. 6b shows a strong increase of the Debye temperature with increasing degree of condensation (Si/N ratio). Note that $\text{SrMg}_3\text{SiN}_4$ and MgSiN_2 have a higher Debye temperature than one would expect

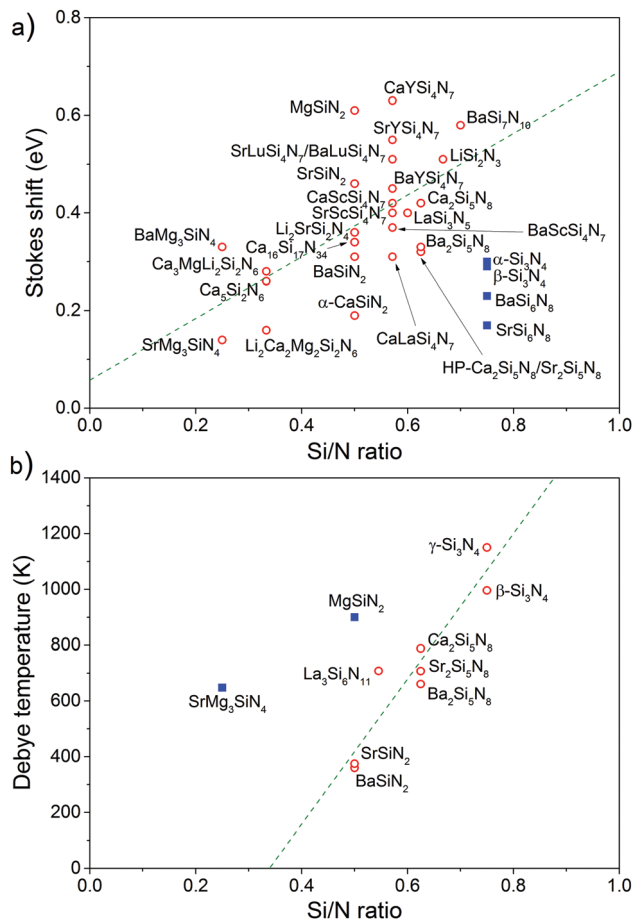


Fig. 6 (a) Eu^{2+} Stokes shift energy and (b) the Debye temperature versus the Si/N ratio (κ) for the Eu^{2+} doped nitridosilicates. The dashed green lines are linear fits through the red data points in order to indicate the trend. More details on the fits can be found in the ESI.†

based on the Si/N ratio, which can be attributed to the fact that Mg forms MgN_4 tetrahedra and should therefore be considered part of the framework, meaning that these compounds actually have a higher degree of condensation than expected from simply the Si/N ratio. The results in Fig. 6b thus confirm an increase of lattice rigidity with increasing degree of condensation.

At first sight, the increase of the Stokes shift with increasing degree of condensation (Si/N ratio), *i.e.* with increasing lattice rigidity, shown in Fig. 6a may be against expectation. A larger Stokes shift is often attributed to more ease of relaxation for Eu^{2+} . So, one might expect that the Stokes shift should actually decrease with increasing Si/N ratio and not increase as shown in Fig. 6a. This suggests that there is a difference between the average lattice rigidity, which indeed increases with increasing degree of condensation, as reflected by a higher Debye temperature, and the local rigidity of the Eu^{2+} ion,⁹⁶ which determines the Stokes shift.

Fig. 7a shows that the Stokes shift tends to increase with increasing average Eu–N distance, where the Eu–N distances have been determined using eqn (5) (Section 3.1). The Stokes shift is relatively small (around 0.15 eV) in $\text{SrMg}_3\text{SiN}_4$: Eu^{2+} and $\text{Li}_2\text{Ca}_2\text{Mg}_2\text{Si}_2\text{N}_6$: Eu^{2+} , which have small Eu–N distances, and

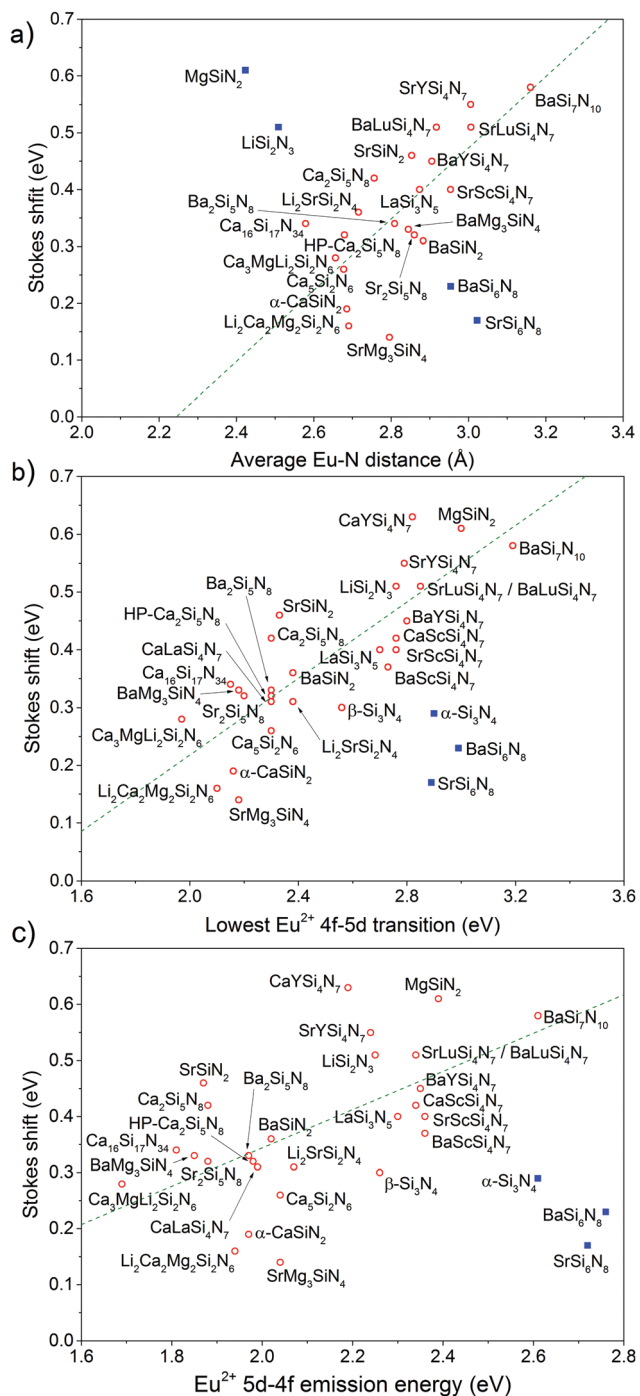


Fig. 7 Eu^{2+} Stokes shift energy versus (a) the average Eu–N distance, (b) the lowest Eu^{2+} 4f–5d transition (E_{fd}), and (c) the Eu^{2+} 5d–4f emission (E_{df}) in the nitridosilicates. The dashed green lines are linear fits through the red data points in order to indicate the trend. More details on the fits can be found in the ESI.† The Stokes shift of $\text{Li}_4\text{Ca}_3\text{Si}_2\text{N}_6:\text{Eu}^{2+}$ is not shown as it is outside the plotted range.

the Stokes shift is relatively large (0.58 eV) in $\text{BaSi}_7\text{N}_{10}:\text{Eu}^{2+}$ with large Eu–N distances. The increase of the Stokes shift with increasing Eu–N distance can be understood by considering that the ligands around Eu will have more ease of relaxation when Eu is on a large site, while a small compact site will have a

higher local rigidity. Exceptions to the trend in Fig. 7a are $(\text{AE})\text{Si}_6\text{N}_8:\text{Eu}^{2+}$ (AE = Sr, Ba), $\text{MgSiN}_2:\text{Eu}^{2+}$ and $\text{LiSi}_2\text{N}_3:\text{Eu}^{2+}$. The higher than expected Stokes shift for $\text{MgSiN}_2:\text{Eu}^{2+}$ and $\text{LiSi}_2\text{N}_3:\text{Eu}^{2+}$ seems to indicate that Eu is not present on the small Mg and Li sites in $\text{MgSiN}_2:\text{Eu}^{2+}$ and $\text{LiSi}_2\text{N}_3:\text{Eu}^{2+}$, as was already concluded in Section 3.1 when discussing the larger than expected E_{fd} (Fig. 4a).

In Fig. 7b, the Stokes shift is plotted versus the energy of the lowest 4f–5d transition (E_{fd}). From the graph, it can clearly be seen that the higher the E_{fd} , the larger the Stokes shift. This automatically follows from the fact that both the Stokes shift (Fig. 7a) and the lowest 4f–5d transition (Fig. 4a) increase with increasing Eu–N distance. Three compounds are clearly an exception: Eu^{2+} doped $\alpha\text{-Si}_3\text{N}_4$, SrSi_6N_8 and BaSi_6N_8 . Here, the Stokes shift is much smaller than expected based on the energy of the 4f–5d transition or based on the Si/N ratio (Fig. 6a). In Eu^{2+} doped SrSi_6N_8 and BaSi_6N_8 , this could be related to the special structural feature of a direct Si–Si bond present in the structure. In the $(\text{AE})\text{Si}_6\text{N}_8$ (AE = Sr, Ba) compounds, as opposed to the other nitridosilicates, not all Si is in the IV+ oxidation state, but 1/3 of the Si atoms are in the III+ oxidation state.⁹⁷ As a result, the average N by Si coordination number (x) is lower ($x = 2.75$) than expected based on the Si/N ratio ($x = 3$).³¹ In $\alpha\text{-Si}_3\text{N}_4$, the Eu^{2+} ion cannot substitute for a large metal ion M and needs to create its own site. In addition, $\alpha\text{-Si}_3\text{N}_4:\text{Eu}^{2+}$ also has a very broad and asymmetrical emission band⁵⁵ indicating that the emission band is a composition of multiple bands due to Eu^{2+} being in different crystalline environments. E_{df} is defined as the maximum of the emission band, but this E_{df} may not correspond to the E_{fd} from Eu^{2+} at the same site, resulting in a smaller Stokes shift value.

Since the Stokes shift increases with increasing Eu^{2+} 4f–5d energy and the Stokes shift is defined as the energy difference between the 4f–5d absorption and 5d–4f emission energy, the Stokes shift also has to increase with increasing 5d–4f emission energy (Fig. 7c). Note that the deviations from the trend line are larger in Fig. 7c than in Fig. 7b (± 0.2 eV versus ± 0.1 eV), which is a consequence of how the Stokes shift is defined.

It was discussed in Section 3.1 that the energy of the Eu^{2+} 4f–5d absorption does not shift significantly by changing AE in the isostructural series $(\text{AE})\text{ScSi}_4\text{N}_7:\text{Eu}^{2+}$ (AE = Ca, Sr, Ba), $(\text{AE})\text{LuSi}_4\text{N}_7:\text{Eu}^{2+}$ (AE = Sr, Ba), $(\text{AE})\text{YSi}_4\text{N}_7:\text{Eu}^{2+}$ (AE = Ca, Sr, Ba) and $(\text{AE})_2\text{Si}_5\text{N}_8:\text{Eu}^{2+}$ (AE = Sr, Ba). However, the Stokes shift may shift by changing the metal ion AE. E_{df} increases, so the Stokes shift decreases, when increasing the size of AE in $(\text{AE})\text{YSi}_4\text{N}_7$. This is in agreement with the mechanism discussed in Section 2.4 that Eu^{2+} tends to shrink at 4f–5d excitation and that this shrinkage is not constrained and even promoted on a small site.⁵⁰ However, the same cannot be concluded for the other isostructural series: here, the Stokes shift is almost constant with differences that are smaller than the uncertainty of 0.1 eV.

The full width at half maximum (FWHM) of the Eu^{2+} emission bands for the Eu^{2+} doped nitridosilicates is listed in Table 1 and shown as a function of the Si/N ratio in Fig. 8a. As the emission of $\text{Ca}_{16}\text{Si}_{17}\text{N}_{34}:\text{Eu}^{2+}$ and $(\text{AE})_2\text{Si}_5\text{N}_8:\text{Eu}^{2+}$ (AE = Ca, Sr, Ba) is from Eu^{2+} on different crystallographic sites, the total

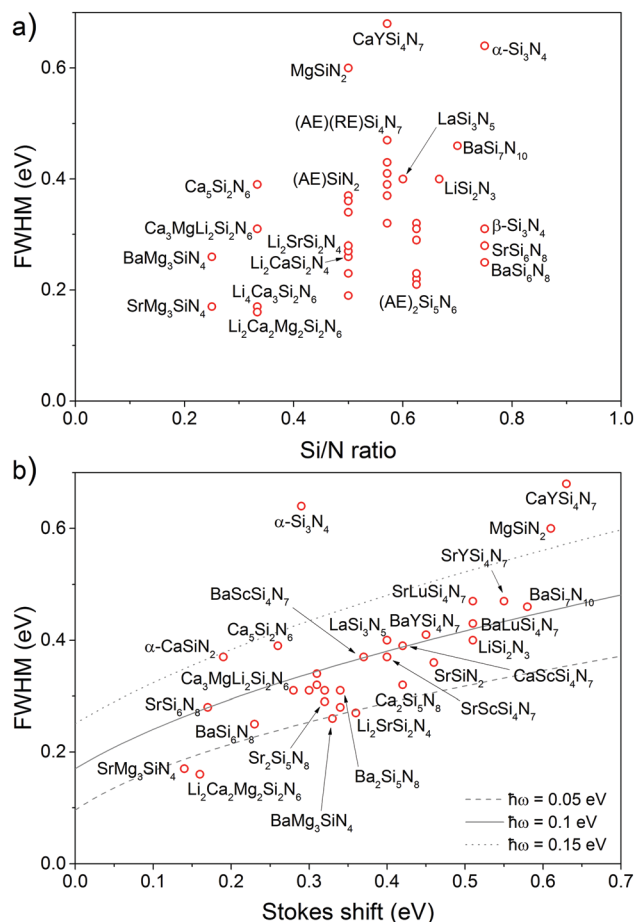


Fig. 8 Full width at half maximum (FWHM) of the Eu^{2+} emission band for the Eu^{2+} doped nitridosilicates versus (a) the Si/N ratio and (b) the Stokes shift. The data points in (a) for $(\text{AE})(\text{RE})\text{Si}_4\text{N}_7:\text{Eu}^{2+}$ (AE = Ca, Sr, Ba; RE = Sc, Y, Lu), $(\text{AE})\text{SiN}_2$ (AE = Ca, Sr, Ba) and $(\text{AE})_2\text{Si}_3\text{N}_8$ (AE = Ca, Sr, Ba) are close together and therefore not indicated with separate labels for each compound. The lines in (b) are given by eqn (4) for a phonon energy $\hbar\omega$ of 0.05 eV, 0.1 eV and 0.15 eV.

emission band is a combination of multiple emission bands at slightly different wavelengths, resulting in an extra broad band. Therefore the FWHM given in Table 1 and Fig. 8 is not the band width of the total emission band, but the FWHM of the individual emission bands of Eu^{2+} at the different sites. Very narrow emission bands (<0.2 eV) are observed for Eu^{2+} doped $\text{SrMg}_3\text{SiN}_4$ and $\text{Li}_2\text{Ca}_2\text{Mg}_2\text{Si}_2\text{N}_6$ with relatively low Si/N ratios. Broad bands are observed for Eu^{2+} doped $\alpha\text{-Si}_3\text{N}_4$ and CaYSi_4N_7 with relatively high Si/N ratios. In general, the FWHM tends to increase with increasing Si/N ratio, but the scattering is very large.

As discussed in Section 2.5, there is a theoretical relation between the FWHM and the Stokes shift, expressed by eqn (4), giving an increase of the FWHM with increasing Stokes shift depending on the phonon energy. In Fig. 8b, this equation is plotted for a phonon energy of 0.05, 0.1 and 0.15 eV. Most of the compounds fall between the 0.05 and 0.15 eV line. Note that the phonon energies reported for $\text{Ca}_2\text{Si}_5\text{N}_8:\text{Eu}^{2+}$ (0.059 eV)⁹⁸ and $\text{Sr}_2\text{Si}_5\text{N}_8:\text{Eu}^{2+}$ (0.052 eV)⁹⁹ are in good agreement with Fig. 8b. One of the clear exceptions in Fig. 8b is $\alpha\text{-Si}_3\text{N}_4:\text{Eu}^{2+}$,

which has a very large FWHM. The broad emission band has a non-Gaussian shape due to the variation of multiple Eu^{2+} environments in $\alpha\text{-Si}_3\text{N}_4:\text{Eu}^{2+}$, resulting in a large distribution of Eu^{2+} 5d–4f emission energies and consequently a large FWHM. Note that the FWHM of $\text{CaYSi}_4\text{N}_7:\text{Eu}^{2+}$ (or actually $\text{Ca}_{0.8}\text{Y}_{1.2}\text{Si}_4\text{N}_{6.8}\text{C}_{0.2}:\text{Eu}^{2+}$), which has a large FWHM in comparison to the other $(\text{AE})(\text{RE})\text{Si}_4\text{N}_7:\text{Eu}^{2+}$ compounds, may be due to a similar reason, considering that it is a disordered structure where nitrogen is partly replaced by carbon and some of the Y^{3+} ions are present on the Ca^{2+} sites,¹⁰⁰ resulting in a large FWHM as a consequence of multiple different Eu^{2+} environments.

According to eqn (4), the FWHM increases with increasing Stokes shift and with increasing phonon energy. Interestingly, the Stokes shift itself tends to increase with increasing Si/N ratio (Fig. 6a) and the phonon energy is also expected to increase with increasing Si/N ratio as the structures become more condensed (Fig. 8b also seems to suggest this). An increase of FWHM with increasing Si/N ratio would therefore be expected. As was mentioned above, this can also be seen from Fig. 8a but the scattering is very large. This is attributed to various local effects on the Eu^{2+} coordination that have a relatively strong influence on the exact width of the emission band, such as site symmetry, Eu by N coordination number, defects, impurities, charge compensation and crystallinity of the sample. These effects may easily cause deviations of 0.1–0.2 eV. As the FWHM only varies by 0.5 eV between all compounds, a 0.1–0.2 eV effect is relatively significant. On the other hand, for example, the absolute variation in the centroid shift is much larger (Fig. 3a, about 1.3 eV), so a 0.1–0.2 eV deviation is therefore relatively less significant.

4. Conclusions and outlook

With decreasing degree of condensation (Si/N ratio) in the $\text{M}_x\text{Si}_y\text{N}_z:\text{Eu}^{2+}$ phosphors, the absorption energy (E_{fd}) between the Eu^{2+} 4f ground state and the lowest 5d state and the emission energy (E_{df}) from the lowest 5d to the 4f ground state both decrease. This is attributed to a lower N by Si coordination number at lower degrees of condensation, which results in fewer electrons on N participating in the bonding with Si. Therefore, with lower Si/N ratios, more electrons become available for bonding with Eu, making the Eu–N bonds more covalent. The higher covalency increases the centroid shift of the Eu^{2+} 5d level (an increased nephelauxetic effect), lowering the 4f–5d energy. The lowering of the N by Si coordination number with decreasing Si/N ratio also results in a decrease of the Eu–N bond lengths. As a consequence, the crystal field splitting tends to become larger, which further lowers the energy of the lowest Eu^{2+} 4f–5d transition. The smaller Eu–N distances with decreasing Si/N ratio also result in an increase of the local rigidity around the Eu^{2+} ion, making the Stokes shift and the band width of the Eu^{2+} 5d–4f emission smaller. In contrast, the average lattice rigidity of the nitridosilicates decreases with lower Si/N ratio due to a lower degree of cross-linking between the SiN_4 tetrahedrons.

Apart from the Si/N ratio, there are also various other factors that are largely independent of the Si/N ratio and have an influence on the Eu^{2+} 4f–5d excitation and 5d–4f emission energy in the Eu^{2+} doped nitridosilicates, such as the Eu^{2+} site symmetry, the Eu by N coordination number, and charge compensation effects. These effects cause deviations from the general trends that are observed when the Si/N ratio is considered the principle parameter. These deviations are relatively large for the emission band width and crystal field splitting, and relatively small for the centroid shift and emission energy.

Compounds with small M cations (Li^+ or Mg^{2+}), such as LiSi_2N_3 and MgSiN_2 , are an exception to some of the general trends as the observed Eu^{2+} 4f–5d energy and Stokes shift are larger than what one would expect based on the short Mg–N and Li–N distances, which is probably an indication that the large Eu^{2+} ion is not located on the small Li and Mg sites. The $(\text{AE})\text{Si}_6\text{N}_8:\text{Eu}^{2+}$ (AE = Sr, Ba) compounds with direct Si–Si bonds also form an exception with their smaller than expected Stokes shift.

The observed trends may be useful for the design of new Eu^{2+} doped nitridosilicate phosphors with specific emission and absorption wavelengths or band widths, and may also be helpful in order to interpret the luminescence data of new Eu^{2+} doped nitridosilicate phosphors. Although the work is limited to the Eu^{2+} doped nitridosilicate compounds, it is believed that the relationships are more general and may also hold for other Eu^{2+} doped lattices that consist of a network of cross-linked TX_4 (T = cation, X = anion) tetrahedra with M cations in between, such as the oxo-silicates, aluminates and phosphates. In addition, similar trends are also expected to apply for the 4f–5d absorption and 5d–4f emission of other lanthanide dopants in these lattices, most notably Ce^{3+} and Yb^{2+} .

Conflicts of interest

There are no conflicts to declare.

Acknowledgements

We acknowledge the valuable input given by Prof. Dr Pieter Dorenbos during the preparation of this manuscript. This research has received funding from the Netherlands Organisation for Scientific Research (NWO) as part of the Joint Research Project on Advanced Materials with the National Natural Science Foundation of China (NSFC).

Notes and references

- R. J. Xie and H. T. Hintzen, *J. Am. Ceram. Soc.*, 2013, **96**, 665–687.
- R. J. Xie and N. Hirosaki, *Sci. Technol. Adv. Mater.*, 2007, **8**, 588–600.
- M. Singh, *Rev. Adv. Mater. Sci.*, 2016, **44**, 134–145.
- R. Mueller-Mach, G. Mueller, M. R. Krames, H. A. Höpfe, F. Stadler, W. Schnick, T. Juestel and P. Schmidt, *Phys. Status Solidi A*, 2005, **202**, 1727–1732.
- R. J. Xie, N. Hirosaki, N. Kimura, K. Sakuma and M. Mitomo, *Appl. Phys. Lett.*, 2007, **90**, 191101.
- S. E. Brinkley, N. Pfaff, K. A. Denault, Z. J. Zhang, H. T. Hintzen, R. Seshadri, S. Nakamura and S. P. DenBaars, *Appl. Phys. Lett.*, 2011, **99**, 241106.
- G. Li, Y. Tian, Y. Zhao and J. Lin, *Chem. Soc. Rev.*, 2015, **44**, 8688–8713.
- R. Withnall, J. Silver, G. R. Fern, T. G. Ireland, A. L. Lipman and B. Patel, *J. Soc. Inf. Disp.*, 2008, **16**, 359–366.
- O. M. ten Kate, M. de Jong, H. T. Hintzen and E. van der Kolk, *J. Appl. Phys.*, 2013, **114**, 084502.
- K. Van den Eeckhout, P. F. Smet and D. Poelman, *Materials*, 2011, **4**, 980–990.
- P. F. Smet, J. Botterman, K. Van den Eeckhout, K. Korthout and D. Poelman, *Opt. Mater.*, 2014, **36**, 1913–1919.
- H. A. Höpfe, H. Lutz, P. Morys, W. Schnick and A. Seilmeier, *J. Phys. Chem. Solids*, 2000, **61**, 2001–2006.
- Y. Q. Li, J. E. J. van Steen, J. W. H. van Krevel, G. Botty, A. C. A. Delsing, F. J. DiSalvo, G. de With and H. T. Hintzen, *J. Alloys Compd.*, 2006, **417**, 273–279.
- C. J. Duan, X. J. Wang, W. M. Otten, A. C. A. Delsing, J. T. Zhao and H. T. Hintzen, *Chem. Mater.*, 2008, **20**, 1597–1605.
- Y. Q. Li, N. Hirosaki, R. J. Xie, T. Takada, Y. Yamamoto, M. Mitomo and K. Shioi, *Int. J. Appl. Ceram. Technol.*, 2010, **7**, 787–802.
- Y. Q. Li, A. C. A. Delsing, R. Metslaar, G. de With and H. T. Hintzen, *J. Alloys Compd.*, 2009, **487**, 28–33.
- Y. Q. Li, G. de With and H. T. Hintzen, *J. Alloys Compd.*, 2004, **385**, 1–11.
- Y. Q. Li, C. M. Fang, G. de With and H. T. Hintzen, *J. Solid State Chem.*, 2004, **177**, 4687–4694.
- T. Kurushima, G. Gundiah, Y. Shimomura, M. Mikami, N. Kijima and A. K. Cheetham, *J. Electrochem. Soc.*, 2010, **157**, J64–J68.
- T. Horikawa, M. Fujitani, H. Hanzawa and K.-I. Machida, *ECS J. Solid State Sci. Technol.*, 2012, **1**, R113–R118.
- W. B. Park, K. H. Son, S. P. Singh and K. S. Sohn, *ACS Comb. Sci.*, 2012, **14**, 537–544.
- K. Uheda, H. Takizawa, T. Endo, H. Yamane, M. Shimada, C. M. Wang and M. Mitomo, *J. Lumin.*, 2000, **87–89**, 967–969.
- Q. Liu and T. Wang, *Phosphors, Up Conversion Nano Particles, Quantum Dots and Their Applications*, Springer, 2017, pp. 343–370.
- Y. Q. Li, A. C. A. Delsing, G. de With and H. T. Hintzen, *Chem. Mater.*, 2005, **17**, 3242–3248.
- K. Uheda, N. Hirosaki, Y. Yamamoto, A. Naito, T. Nakajima and H. Yamamoto, *Electrochem. Solid-State Lett.*, 2006, **9**, H22–H25.
- J. W. H. van Krevel, J. W. T. van Rutten, H. Mandal, H. T. Hintzen and R. Metselaar, *J. Solid State Chem.*, 2002, **165**, 19–24.
- R. J. Xie, N. Hirosaki, M. Mitomo, Y. Yamamoto, T. Suehiro and K. Sakuma, *J. Phys. Chem. B*, 2004, **108**, 12027–12031.
- N. Hirosaki, R. J. Xie, K. Kimoto, T. Sekiguchi, Y. Yamamoto, T. Suehiro and M. Mitomo, *Appl. Phys. Lett.*, 2005, **86**, 211905.

- 29 M. Mikami, S. Shimooka, K. Uheda, H. Imura and N. Kijima, *Key Eng. Mater.*, 2009, **403**, 11–14.
- 30 K. Shioi, N. Hirotsaki, R. J. Xie, T. Takeda and Y. Q. Li, *J. Mater. Sci.*, 2008, **43**, 5659–5661.
- 31 O. M. ten Kate, Z. Zhang and H. T. Hintzen, *J. Mater. Chem. C*, 2017, **44**, 11504–11514.
- 32 M. Zeuner, S. Pagano and W. Schnick, *Angew. Chem., Int. Ed. Engl.*, 2011, **50**, 7754–7775.
- 33 X. H. He, N. Lian, J. H. Sun and M. Y. Guan, *J. Mater. Sci.*, 2009, **44**, 4763–4775.
- 34 T. Wang, Z. G. Xia, Q. C. Xiang, S. Q. Qin and Q. L. Liu, *J. Lumin.*, 2015, **166**, 106–110.
- 35 S. Wang, Z. Song, Y. Kong, Z. Xia and Q. Liu, *J. Lumin.*, 2018, **194**, 461–466.
- 36 H. Onuma, R. Nagumo, R. Miura, A. Suzuki, H. Tsuboi, N. Hatakeyama, H. Takaba and A. Miyamoto, *J. Ceram. Process. Res.*, 2013, **14**, S48–S51.
- 37 Y. Jia, A. Miglio, S. Poncé, X. Gonze and M. Mikami, *Phys. Rev. B: Condens. Matter Mater. Phys.*, 2016, **93**, 155111.
- 38 Z. Wang, I.-H. Chu, F. Zhou and S. P. Ong, *Chem. Mater.*, 2016, **28**, 4024–4031.
- 39 P. Dorenbos, *J. Lumin.*, 2003, **104**, 239–260.
- 40 P. Dorenbos, *J. Lumin.*, 2008, **128**, 578–582.
- 41 P. Dorenbos, *J. Phys.: Condens. Matter*, 2003, **15**, 4797–4807.
- 42 P. Dorenbos, *Phys. Rev. B: Condens. Matter Mater. Phys.*, 2012, **85**, 165107.
- 43 F. Gao and S. Zhang, *J. Phys. Chem. Solids*, 1997, **58**, 1991–1994.
- 44 P. Dorenbos, *J. Lumin.*, 2013, **136**, 122–129.
- 45 C. A. Morrison, *J. Chem. Phys.*, 1980, **72**, 1001–1002.
- 46 P. Dorenbos, *Phys. Rev. B: Condens. Matter Mater. Phys.*, 2002, **65**, 235110.
- 47 P. Dorenbos, *J. Alloys Compd.*, 2002, **341**, 156–159.
- 48 P. Dorenbos, *J. Phys.: Condens. Matter*, 2003, **15**, 575–594.
- 49 J. Verwey and G. Blasse, *Mater. Chem. Phys.*, 1990, **25**, 91–103.
- 50 G. Blasse, *Handbook on the Physics and Chemistry of Rare Earths*, Chemistry and Physics of R-activated Phosphors, 1979, ch. 34, vol. 4, pp. 237–274.
- 51 B. Henderson and G. Imbusch, *Optical Spectroscopy of Inorganic Solids*, Oxford University Press, 2006.
- 52 X. Huang, *Nat. Photonics*, 2014, **8**, 748–749.
- 53 Q. Wu, J. Ding, Y. Li, X. Wang and Y. Wang, *J. Lumin.*, 2017, **186**, 144–151.
- 54 O. M. ten Kate, H. T. Hintzen and E. van der Kolk, *J. Phys.: Condens. Matter*, 2014, **26**, 385502.
- 55 Y. Q. Li, N. Hirotsaki, R. J. Xie, T. Takeda and M. Mitomo, *J. Lumin.*, 2010, **130**, 1147–1153.
- 56 N. Hirotsaki, *US Pat.*, 8147715, U.S. Patent and Trademark Office, Washington, DC, 2012.
- 57 F. Yu, J. Yang, A. C. Delsing and H. T. Hintzen, *J. Lumin.*, 2010, **130**, 2298–2304.
- 58 J. Y. Ding, Q. S. Wu, Y. Y. Li, Q. Long, C. Wang and Y. H. Wang, *J. Am. Ceram. Soc.*, 2015, **98**, 2523–2527.
- 59 Y. Q. Li, N. Hirotsaki, R. J. Xie, T. Takeka and M. Mitomo, *J. Solid State Chem.*, 2009, **182**, 301–311.
- 60 T. Wang, Q. Xiang, Z. Xia, J. Chen and Q. Liu, *Inorg. Chem.*, 2016, **55**, 2929–2933.
- 61 Q. S. Wu, J. Y. Ding, C. Wang, Y. Y. Li, X. C. Wang, A. J. Mao and Y. H. Wang, *RSC Adv.*, 2015, **5**, 31255–31261.
- 62 Q. S. Wu, Y. Y. Li, X. C. Wang, Z. Y. Zhao, C. Wang, H. Li, A. J. Mao and Y. H. Wang, *RSC Adv.*, 2014, **4**, 39030–39036.
- 63 G. P. Dubrovskii, A. M. Zykov and B. V. Chernovets, *Inorg. Mater.*, 1981, **17**, 1059–1063.
- 64 G. K. Gaido, G. P. Dubrovskii and A. M. Zykov, *Izv. Akad. Nauk SSSR, Neorg. Mater.*, 1974, **10**, 485.
- 65 Z. Lenčič, A. Czimerová, M. Vyležiková, P. Šajgalík and Z. Jonšta, *Processing and Properties of Advanced Ceramics*, Slovak Academy of Sciences, 2016, pp. 98–102.
- 66 J.-J. Huang, H.-C. Kuo and S.-C. Shen, *Nitride Semiconductor Light-Emitting Diodes (LEDs): Materials, Technologies and Applications*, Woodhead Publishing, 2014.
- 67 J. Huang, T. Jiang, N. Yao, H. Li and X. Xu, *Asian J. Chem.*, 2015, **27**, 938–940.
- 68 S. S. Lee, S. Lim, S.-S. Sun and J. F. Wager, *Proc. SPIE*, 1997, **3241**, 75–83.
- 69 H. Chen, J. Ding, X. Ding, X. Wang, Y. Cao, Z. Zhao and Y. Wang, *Inorg. Chem.*, 2017, **56**, 10904–10913.
- 70 O. M. ten Kate, Z. Zhang, P. Dorenbos, H. T. Hintzen and E. van der Kolk, *J. Solid State Chem.*, 2013, **197**, 209–217.
- 71 W. T. Chen, H. S. Sheu, R. S. Liu and J. P. Attfield, *J. Am. Chem. Soc.*, 2012, **134**, 8022–8025.
- 72 H. L. Li, R. J. Xie, N. Hirotsaki, T. Takeda and G. H. Zhou, *Int. J. Appl. Ceram. Technol.*, 2009, **6**, 459–464.
- 73 S. R. Römer, C. Braun, O. Oeckler, P. J. Schmidt, P. Kroll and W. Schnick, *Chem. – Eur. J.*, 2008, **14**, 7892–7902.
- 74 L. Chen, R. H. Liu, W. D. Zhuang, Y. H. Liu, Y. S. Hu, X. L. Ma and B. Hu, *J. Rare Earths*, 2016, **34**, 30–35.
- 75 X. Piao, K. I. Machida, T. Horikawa and H. Hanzawa, *Appl. Phys. Lett.*, 2007, **91**, 041908.
- 76 J. L. Qin, H. R. Zhang, B. F. Lei, H. W. Dong, Y. L. Liu, J. X. Meng, M. T. Zheng and Y. Xiao, *J. Lumin.*, 2014, **152**, 230–233.
- 77 K. Ueda, H. Yamane, T. Nagura and T. Miyazaki, *Japanese Pat.*, JP2015-196717, 2015.
- 78 S. Schmiechen, H. Schneider, P. Wagatha, C. Hecht, P. J. Schmidt and W. Schnick, *Chem. Mater.*, 2014, **26**, 2712–2719.
- 79 S. Schmiechen, P. Strobel, C. Hecht, T. Reith, M. Siegert, P. J. Schmidt, P. Huppertz, D. Wiechert and W. Schnick, *Chem. Mater.*, 2015, **27**, 1780–1785.
- 80 Y. Zhou, Y. I. Yoshizawa, K. Hirao, Z. Lenčič and P. Šajgalík, *J. Eur. Ceram. Soc.*, 2011, **31**, 151–157.
- 81 O. M. ten Kate, H. T. Hintzen, P. Dorenbos and E. van der Kolk, *J. Mater. Chem.*, 2011, **21**, 18289–18294.
- 82 M. Zeuner, *Molekulare Precursoren und neue Synthesestrategien zu Nitridosilicaten und deren Verwendung für phosphorkonvertierte LEDs*, PhD Thesis, Ludwig-Maximilians-Universität München, 2009.
- 83 T. M. Tolhurst, P. Strobel, P. J. Schmidt, W. Schnick and A. Moewes, *J. Phys. Chem. C*, 2017, **121**, 14296–14301.
- 84 P. Strobel, V. Weiler, C. Hecht, P. J. Schmidt and W. Schnick, *Chem. Mater.*, 2017, **29**, 1377–1383.
- 85 C. Poesl and W. Schnick, *Chem. Mater.*, 2017, **29**, 3778–3784.

- 86 D. Porob, N. Karkada, N. P. Kumar and A. Setlur, *ECS Trans.*, 2012, **41**, 27–38.
- 87 X. C. Wang, T. Seto, Z. Y. Zhao, Y. Y. Li, Q. S. Wu, H. Li and Y. H. Wang, *J. Mater. Chem. C*, 2014, **2**, 4476–4481.
- 88 R. J. Xie and N. Hirotsaki, *Japanese Pat.*, JP2009-096823, 2009.
- 89 P. Dorenbos, *ECS J. Solid State Sci. Technol.*, 2013, **2**, R3001–R3011.
- 90 R. T. Shannon, *Acta Crystallogr., Sect. A: Cryst. Phys., Diffr., Theor. Gen. Crystallogr.*, 1976, **32**, 751–767.
- 91 J. Jiang, H. Lindelov, L. Gerward, K. Ståhl, J. Recio, P. Morisánchez, S. Carlson, M. Mezouar, E. Dooryhee and A. Fitch, *Phys. Rev. B: Condens. Matter Mater. Phys.*, 2002, **65**, 161202.
- 92 N. C. George, A. Birkel, J. Brgoch, B. C. Hong, A. A. Mikhailovsky, K. Page, A. Llobet and R. Seshadri, *Inorg. Chem.*, 2013, **52**, 13730–13741.
- 93 X. Huang, J. Sun, X. Sheng, Y. Huang and L. Ning, *J. Lumin.*, 2017, **185**, 187–191.
- 94 R. J. Bruls, H. T. Hintzen, G. de With and R. Metselaar, *J. Eur. Ceram. Soc.*, 2001, **21**, 263–268.
- 95 J. Brgoch, S. P. DenBaars and R. Seshadri, *J. Phys. Chem. C*, 2013, **117**, 17955–17959.
- 96 K. A. Denault, J. Brgoch, S. D. Kloß, M. W. Gaultois, J. Siewenie, K. Page and R. Seshadri, *ACS Appl. Mater. Interfaces*, 2015, **7**, 7264–7272.
- 97 F. Stadler, O. Oeckler, J. Senker, H. A. Höpfe, P. Kroll and W. Schnick, *Angew. Chem., Int. Ed. Engl.*, 2005, **44**, 567–570.
- 98 X. D. Wei, L. Y. Cai, F. C. Lu, X. L. Chen, X. Y. Chen and Q. L. Liu, *Chin. Phys. B*, 2009, **18**, 3555–3562.
- 99 A. Lazarowska, S. Mahlik, M. Grinberg, C. W. Yeh and R. S. Liu, *Opt. Mater.*, 2014, **37**, 734–739.
- 100 K. Liddell, D. P. Thompson and S. J. Teat, *J. Eur. Ceram. Soc.*, 2005, **25**, 49–54.